

Supporting Information

Complete charge separation provoked by full cation encapsulation in the radical mono- and di-anion of 5,6:11,12-di-*o*-phenylenetetracene

Tobias Wombacher, Richard Goddard, Christian W. Lehmann and Jörg J. Schneider

Content

1 Single crystal X-ray structure analysis	S2
1.1 Single crystal structure analysis of DOPT Potassium bis(benzo-15-crown-5-ether) 1	S2
1.2 Single crystal structure analysis of DOPT Dipotassium bis(benzo-15-crown-5-ether) 2	S4
2 Graphical details on the figures given in the manuscript	S6
3 Deformation of the carbon skeleton in solvent-separated anions of DOPT	S7
3.1 Referencing to neutral DOPT	S7
3.2 Detailed structural changes in DOPT Potassium bis(benzo-15-crown-5-ether) 1	S8
3.3 Detailed structural changes in DOPT Dipotassium bis(benzo-15-crown-5-ether) 2	S9
4 Comparison of 6 and 7 to the <i>full naked</i> anion of DOPT 2	S10
5. Experimental details	S11
6. Literature	S11

1 Single crystal X-ray structure analysis

1.1 Single crystal structure analysis of DOPT Potassium bis(benzo-15-crown-5-ether) **1**

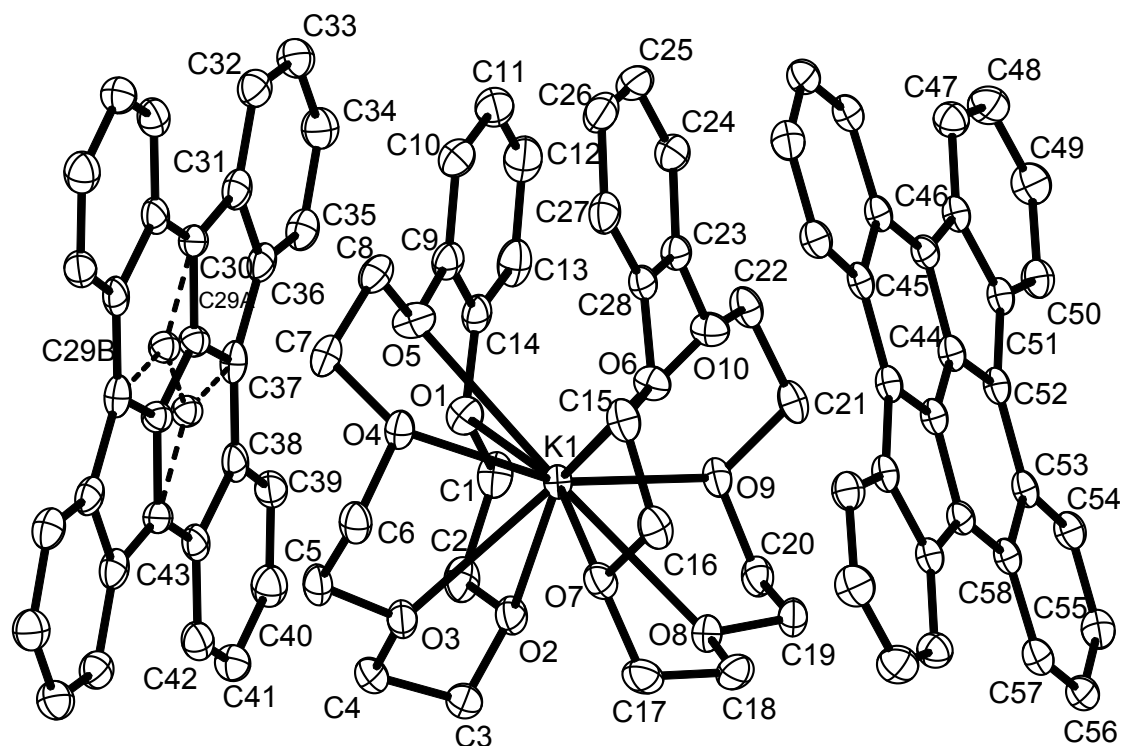


Figure S 1. The molecular structure of **1**. H atoms have been removed for clarity.

X-ray Crystal Structure Analysis of 1: $C_{58}H_{56}KO_{10}$, $M_r = 952.12 \text{ g} \cdot \text{mol}^{-1}$, dark-green prism, crystal size $0.070 \times 0.194 \times 0.234 \text{ mm}^3$, triclinic, space group $P \bar{1}$ (No 2), $a = 11.0923(3) \text{ \AA}$, $b = 13.0606(3) \text{ \AA}$, $c = 16.7307(4) \text{ \AA}$, $\alpha = 82.9084(10)^\circ$, $\beta = 80.2410(9)^\circ$, $\gamma = 76.9312(10)^\circ$, $V = 2317.7(1) \text{ \AA}^3$, $T = 100(2) \text{ K}$, $Z = 2$, $D_{\text{calc}} = 1.364 \text{ g} \cdot \text{cm}^3$, $\lambda = 1.54178 \text{ \AA}$, $\mu(\text{Cu-K}\alpha) = 1.527 \text{ mm}^{-1}$, analytical absorption correction ($T_{\text{min}} = 0.77995$, $T_{\text{max}} = 0.91280$), Bruker-AXS Proteum X8 diffractometer, $2.690 < \theta < 67.489^\circ$, 55453 measured reflections, 8049 independent reflections, 7238 reflections with $I > 2\sigma(I)$, $R_{\text{int}} = 0.0358$. The structure was solved by direct methods (*SHELXS*) and refined by full-matrix least-squares (*SHELXL*) against F^2 to $R_1 = 0.0319$ [$I > 2\sigma(I)$], $wR_2 = 0.0788$, 622 parameters.

INTENSITY STATISTICS FOR DATASET

Resolution	#Data	#Theory	%Complete	Redundancy	Mean I	Mean I/s	Rmerge	Rsigma
Inf - 3.45	121	121	100.0	4.03	36.9	47.00	0.0232	0.0179
3.45 - 2.28	283	283	100.0	6.99	14.9	60.82	0.0286	0.0143
2.28 - 1.81	417	417	100.0	8.31	9.5	58.28	0.0274	0.0123
1.81 - 1.58	406	406	100.0	7.38	6.2	46.97	0.0252	0.0145
1.58 - 1.44	390	390	100.0	6.81	4.7	39.58	0.0286	0.0169
1.44 - 1.34	399	399	100.0	11.09	2.9	42.17	0.0422	0.0171
1.34 - 1.26	404	404	100.0	11.07	3.5	41.60	0.0394	0.0169
1.26 - 1.19	450	453	99.3	10.52	3.8	40.35	0.0394	0.0169
1.19 - 1.14	398	402	99.0	8.97	4.4	37.36	0.0345	0.0177
1.14 - 1.10	363	369	98.4	8.15	3.9	33.93	0.0317	0.0201
1.10 - 1.06	440	444	99.1	7.94	2.6	29.41	0.0419	0.0238
1.06 - 1.02	469	482	97.3	7.50	2.1	27.10	0.0495	0.0273
1.02 - 0.99	422	431	97.9	7.25	1.7	23.29	0.0568	0.0303
0.99 - 0.97	316	326	96.9	6.92	1.6	23.01	0.0620	0.0313
0.97 - 0.94	491	512	95.9	5.93	1.4	19.31	0.0677	0.0370
0.94 - 0.92	372	389	95.6	3.97	1.4	16.05	0.0627	0.0457
0.92 - 0.90	421	438	96.1	3.94	1.5	16.36	0.0569	0.0416
0.90 - 0.88	418	444	94.1	3.52	1.5	16.25	0.0638	0.0444
0.88 - 0.86	481	512	93.9	3.25	1.2	14.94	0.0729	0.0491
0.86 - 0.85	257	282	91.1	2.89	1.0	12.83	0.0820	0.0556
0.85 - 0.83	331	458	72.3	1.60	0.8	9.34	0.0755	0.0758

0.93 - 0.83	2106	2341	90.0	3.12	1.3	14.53	0.0654	0.0489
Inf - 0.83	8049	8362	96.3	6.63	3.9	30.58	0.0356	0.0206

One of the independent 5,6:11,12-di-*o*-phenylenetetracene anion radicals is partially rotationally disordered [11.5(7)%]. This was manifest as disorder of C29 over two positions, C29A and C29B. C29A and C29B were refined with isotropic atomic displacement parameters. H atoms were refined using a riding model, $S = 0.969$, residual electron density 0.18 / -0.26 e Å⁻³. **CCDC-1820791**.

1.2 Single crystal structure analysis of DOPT Di-potassium bis(benzo-15-crown-5-ether) **2**

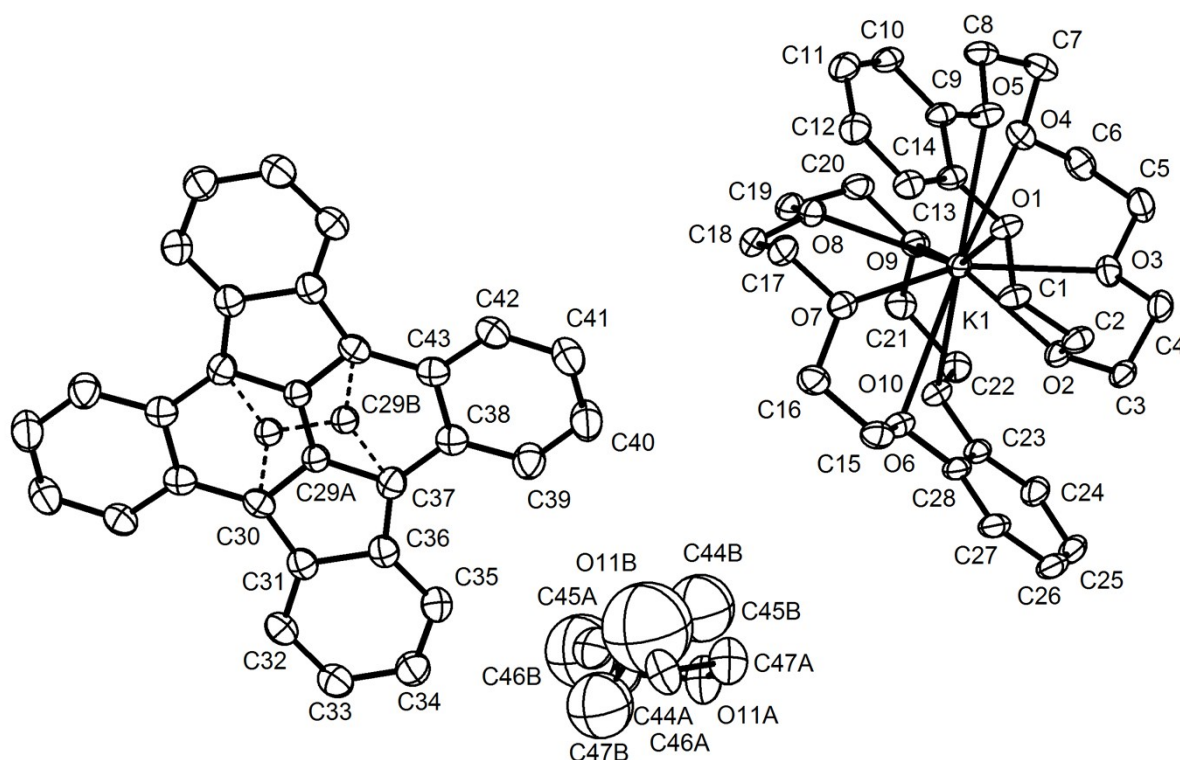


Figure S 2. The molecular structure of **2**. The crystal contains tetrahydrofuran partially disordered over two positions with a relative refined occupancy of 0.621(4):0.379(4). H atoms have been removed for clarity.

X-ray Crystal Structure Analysis of 2: $C_{94}H_{112}K_2O_{22}$, $M_r = 1672.03 \text{ g} \cdot \text{mol}^{-1}$, red-black plate, crystal size $0.15 \times 0.24 \times 0.28 \text{ mm}^3$, triclinic, space group $P\bar{1}$ (No 2), $a = 12.746(7) \text{ \AA}$, $b = 13.528(3) \text{ \AA}$, $c = 13.986(4) \text{ \AA}$, $\alpha = 117.713(4)^\circ$, $\beta = 94.525(6)^\circ$, $\gamma = 96.238(5)^\circ$, $V = 2099.2(13) \text{ \AA}^3$, $T = 100(2) \text{ K}$, $Z = 1$, $D_{\text{calc}} = 1.323 \text{ g} \cdot \text{cm}^3$, $\lambda = 0.71073 \text{ \AA}$, $\mu(Mo-K\alpha) = 0.189 \text{ mm}^{-1}$, analytical absorption correction ($T_{\text{min}} = 0.92526$, $T_{\text{max}} = 0.97842$), Bruker-AXS Enraf-Nonius μS Kappa Mach2 Apex-II diffractometer, $1.625 < \theta < 34.478^\circ$, 75133 measured reflections, 17651 independent reflections, 13585 reflections with $I > 2\sigma(I)$, $R_{\text{int}} = 0.0358$. The structure was solved by direct methods (*SHELXS*) and refined by full-matrix least-squares (*SHELXL*) against F^2 to $R_1 = 0.0564$ [$I > 2\sigma(I)$], $wR_2 = 0.1706$, 552 parameters. Several low-angle reflections were shadowed by the beamstop and removed from the data set before the final refinement cycles.

INTENSITY STATISTICS FOR DATASET

Resolution	#Data	#Theory	%Complete	Redundancy	Mean I	Mean I/s	Rmerge	Rsigma
Inf - 2.55	265	265	100.0	6.33	42.9	68.18	0.0242	0.0135
2.55 - 1.70	637	637	100.0	6.35	14.5	55.58	0.0229	0.0140
1.70 - 1.35	890	890	100.0	6.33	6.2	46.50	0.0259	0.0158
1.35 - 1.18	884	885	99.9	6.06	5.1	41.31	0.0287	0.0173
1.18 - 1.07	905	905	100.0	5.55	4.3	35.81	0.0328	0.0198
1.07 - 0.99	956	956	100.0	5.18	2.4	26.58	0.0392	0.0257
0.99 - 0.94	766	766	100.0	4.83	1.7	21.33	0.0514	0.0328
0.94 - 0.89	925	925	100.0	4.62	1.6	20.19	0.0508	0.0358
0.89 - 0.85	928	928	100.0	4.38	1.4	17.61	0.0589	0.0408
0.85 - 0.82	817	817	100.0	4.19	1.1	14.10	0.0701	0.0517
0.82 - 0.79	918	918	100.0	4.02	0.9	12.14	0.0806	0.0618
0.79 - 0.76	1112	1112	100.0	3.85	0.7	9.94	0.0903	0.0765
0.76 - 0.74	851	851	100.0	3.73	0.8	9.94	0.0909	0.0755
0.74 - 0.72	931	931	100.0	3.54	0.7	8.91	0.1013	0.0870
0.72 - 0.70	1022	1022	100.0	3.46	0.7	8.33	0.1060	0.0933
0.70 - 0.69	582	583	99.8	3.32	0.6	7.68	0.1163	0.0998
0.69 - 0.67	1208	1212	99.7	3.23	0.6	7.10	0.1234	0.1137
0.67 - 0.66	712	718	99.2	3.11	0.5	5.90	0.1465	0.1381
0.66 - 0.65	670	676	99.1	3.07	0.5	5.68	0.1505	0.1460
0.65 - 0.63	1672	1777	94.1	2.73	0.4	4.49	0.1938	0.1873

0.73 - 0.63	6349	6471	98.1	3.13	0.5	6.55	0.1314	0.1234
Inf - 0.63	17651	17774	99.3	4.23	2.7	18.59	0.0352	0.0289

The solvent tetrahydrofuran is partially disordered [37.9(4)%], so is the 5,6:11,12-di-*o*-phenylenetetracene ligand [12.3(3)%] based on refinement of the atom C29 split over two positions: C29A and C29B were refined with isotropic atomic displacement parameters which were constrained to be equal). The atoms of the minor component of the partially disordered solvent tetrahydrofuran molecule were refined with isotropic atomic displacement parameters. Two low-angle weak reflections (0 0 4) and (1 -2 1) at respectively 3.06 and 6.21 Å resolution exhibited calculated F_o^2 significantly higher than F_c^2 . The ratios error/esd were respectively 11.67 and 11.18. We have no explanation for this other than the low angle reflections were measured with a high redundancy resulting in lower estimated standard uncertainties for these intensities and higher than expected $(F_o^2 - F_c^2)/\text{SigmaW}$ values. H atoms were refined using a riding model, $S = 1.031$, residual electron density 0.89 / -0.43 e Å⁻³. **CCDC-1820792**.

2 Graphical details on the figures given in the manuscript

All figures are based on the experimental crystal structure data of the compounds¹⁻³ and are presented without further modifications. The depiction given in Fig. 7a of the manuscript on the local bond lengths variation (Δd_{C-C}) in **1** and **2** was accomplished via reasoned grouping of the experimental bond length values of all charged π -perimeters ($[L_{DOPT}^{\bullet+}]$ in **1**, $[L_{DOPT}^{2-}]$ in **2 - 7**). The detailed allocation of the relevant bond length range (C-C-bonds in **1 - 7** vary within: ca. 130 - 150 pm) to the herein depicted bond-radius is presented in the following Table S 1. Accordingly, the particular thickness of the grouped bonds was assigned in steps from 80 to 5 pm to visualize significant variations along the π -perimeter.

Table S 1. Allocation of the bond length range to the particular bond-radius, as used in Fig. 7a of the manuscript. Within the limit of error of the obtained crystallographic data, the grouping facilitates a contrasting juxtaposition along the alkaline metal series of compounds **1** to **7**.

bond length range (pm)	bond-radius (pm)
130 - 133	80
133 - 136	60
136 - 137	50
137 - 138	45
138 - 139	42
139 \geq 140	38
140 - 141	35
141 - 142	30
142 \geq 143	20
143 - 144	15
144 - 145	10
145 - 146	9
146 - 147	8
147 - 148	7
148 - 150	5

The employed radii of the particular alkaline metals are listed in the following Table S2 and are intentional below the ionic radii as e.g., reported by Shannon⁴. This is due to clarity reasons.

Table S 2. Used ion-radii (pm) for drawings of the alkaline metal ions.

alkaline metal ion	ion-radius (pm)
Li ⁺	44
Na ⁺	54
K ⁺	66
Rb ⁺	75
Cs ⁺	80

The utilized color-coding in red and blue refers to the predicted electron density of newly occupied LUMO of neutral L_{DOPT} . Thus, a direct comparison between actual increase in local electron density (decrease in bond length = bond thickening) based on the experimental results and the predicted positions according to the DFT calculations is possible by checking against the HOMO.

3 Deformation of the carbon skeleton in solvent-separated anions of DOPT

3.1 Referencing to neutral DOPT

The change of the carbon skeleton is presented in relation to the used starting material of monoclinic $C 2/c$ polymorph of neutral L_{DOPT} selectively obtained following our recently published wet-chemical synthesis route^{3,5}. Deviations (Δd_{c-c}) are given in $\pm pm$ for all solvent-separated ion-pairs of anionic DOPT **1-5** including all crystallographic different modifications A and B found within the crystalline lattice (Table S 2). For clarity reasons, even for the non-symmetric carbon skeletons in $\{[(DME-\kappa^2O)_3Li^+]_2(L_{DOPT}^{2-})\}$ **3**² and $\{[(DME-\kappa^2O)_3Na^+]_2(L_{DOPT}^{2-})\}$ **4**², singly one quarter of the symmetric DOPT plane is regarded according to Fig. S 3.

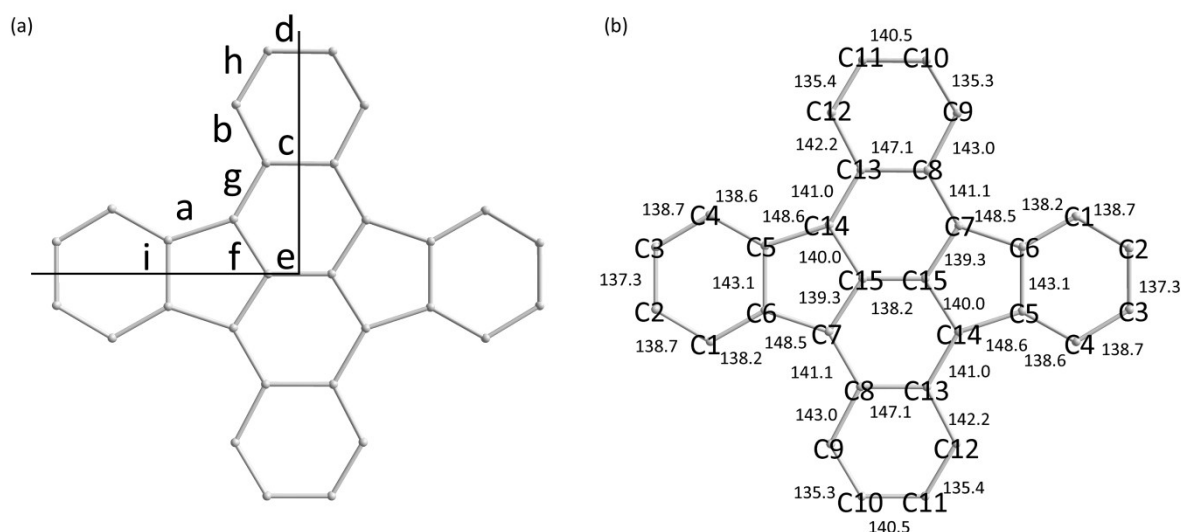


Figure S 3. (a) Bond allocation a-i for easy comparison of all anionic compounds to the $C 2/c$ polymorph of neutral DOPT. The peripheral phenylenes (Pn_{per}) are almost unaffected and were omitted for clarity. (b) Bond length distribution along the neutral carbon skeleton of L_{DOPT} .³ The atomic numbering follows strictly the atom code from the crystallographic data (CCDC 1448442) This data can be obtained free of charge from The Cambridge Crystallographic Data Centre via www.ccdc.cam.ac.uk/data_request/cif.

Table S 3. Summarized variation of the carbon skeletons in all solvent-separated compounds **1 - 5** including the reference values of neutral DOPT (L_{DOPT}) in its monoclinic $C 2/c$ polymorph³. The bond-allocation a-i follows Fig. S 3a. The steady increase resp. decrease of the recorded bond length is highlighted in green-scale (mono-anion **1**: light green; dianion **2**: dark green). Compliance with the changes in bond length in compound **2** is marked in dark green. Significant deviations are highlighted in orange. The observed range in bond length deviation (Δd_{c-c}) is highlighted in yellow. Values are given in $\pm pm$.

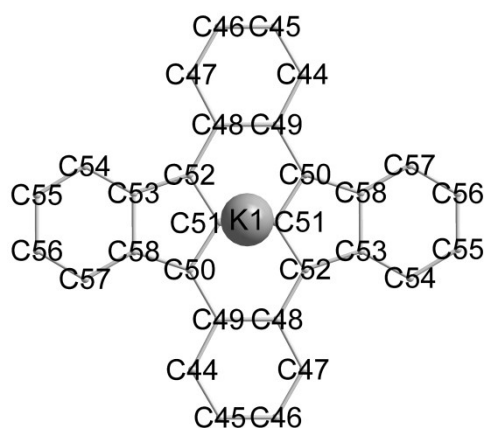
\rightarrow compound	L_{DOPT}^{θ}	1	2	3 ²	4 ²	5 ²		
\rightarrow type	($C 2/c$)			(A)	(B)	(A)	(B)	
\rightarrow ion(s)	—	1K ⁺	2K ⁺	2Li ⁺	2Li ⁺	2Na ⁺	2Na ⁺	2Na ⁺
\rightarrow ligands	—	B15C5	B15C5	DME	DME	DME	DME	diglyme
\downarrow bond								
a	148.6	-2.1 -2.4	-4.1 -4.4	-5.1 \leftrightarrow -6.0	-4.7 \leftrightarrow -6.3	-3.7 \leftrightarrow -5.8	-4.5 \leftrightarrow -5.6	-4.7 -4.8
b	142.2 143.0	-1.1 -1.4	-1.2 -2.2	-1.0 \leftrightarrow -2.1	-1.6 \leftrightarrow -2.0	-2.2 \leftrightarrow -4.6	-2.8 \leftrightarrow -4.0	-1.5 -2.1
c	147.1	-0.4	-0.8	-2.8 -2.9	-2.2 -2.9	-0.7 -1.5	-0.5 -1.1	-1.1
d								
e								
f								
g								
h								
i								

140.5	-0.6	-0.7	-2.1 -4.0	-2.1 -3.5	-1.3 -2.3	-2.4 -2.5	-1.1
138.2	±0.0	-0.1	-0.3	-0.4	+1.2	+1.2	+0.6
139.3 140.0	-0.1 +0.9	+1.1 +2.9	-0.2↔+1.5	±0.0↔+2.3	-1.2↔+0.6	-0.2↔-2.4	+0.7 +1.4
141.0 141.1	+2.2 +2.3	+3.5 +3.7	+4.1↔+4.6	+3.2↔+5.4	+1.9↔+2.9	+2.9↔+3.2	+3.7 +4.0
135.3 135.4	+2.2 +2.2	+3.6 +4.0	+2.4↔+4.3	+2.0↔+3.8	+0.8↔+3.0	+0.9↔+2.9	+3.9 +3.9
143.1	+2.2	+4.1	+4.0 +4.3	+3.5 +5.5	+2.0 +3.9	+2.8 +4.2	+4.2

3.2 Detailed structural changes in DOPT Potassium bis(benzo-15-crown-5-ether) **1**

A detailed view is given below on the experimentally obtained bond length values ($d(\text{C}-\text{C})$) along the charged π -perimeter [L_{DOPT}^*] of compound **1**, together with its deviation ($\Delta d_{\text{C}-\text{C}}$) from the neutral state of L_{DOPT} in its used C 2/c polymorph directly obtained from wet-chemical synthesis of the PAH^{3,5}.

(a)



(b)

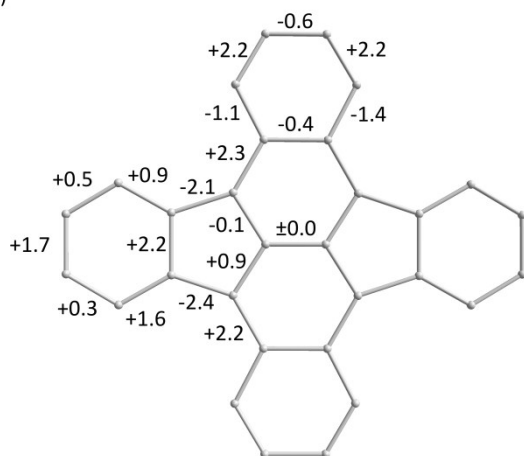


Table S 4. (top) Bond length values of compound **1** for the charged carbon skeleton in [L_{DOPT}^*] given in pm. Deviations are omitted for clarity and can be found in the corresponding X-ray structural data (CCDC 1820791). (bottom) Side view on [L_{DOPT}^*] in compound **1**.

C(A)-C(B)	$d(\text{C}-\text{C})$	C(A)-C(B)	$d(\text{C}-\text{C})$
C44 - C45	137.5	C51 - C52	139.9
C44 - C49	141.6	C51 - C51	138.2
C45 - C46	139.9	C52 - C53	146.5
C46 - C47	137.6	C53 - C58	145.3
C47 - C48	141.1	C53 - C54	139.5
C48 - C49	146.7	C54 - C55	139.2
C48 - C52	143.3	C55 - C56	139.0
C49 - C50	143.3	C57 - C58	139.8
C50 - C58	146.1	C57 - C56	139.0
C50 - C51	140.2		



Figure S 4. (a) Atom numbering scheme of compound **1** based on the allocated atom symbols of the crystal structure data set. (b) Relative change ($\Delta d_{\text{C}-\text{C}}$) in bond length given in $\pm\text{pm}$ referenced to the used starting compound (C 2/c polymorph of neutral $\text{L}_{\text{DOPT}}^{\text{0}}$)³.

An additional visualization of bond length distribution is given below in Fig. S 5. Thick drawing of a C-C bond corresponds to small bond length resp. increased electron concentration and vice versa.

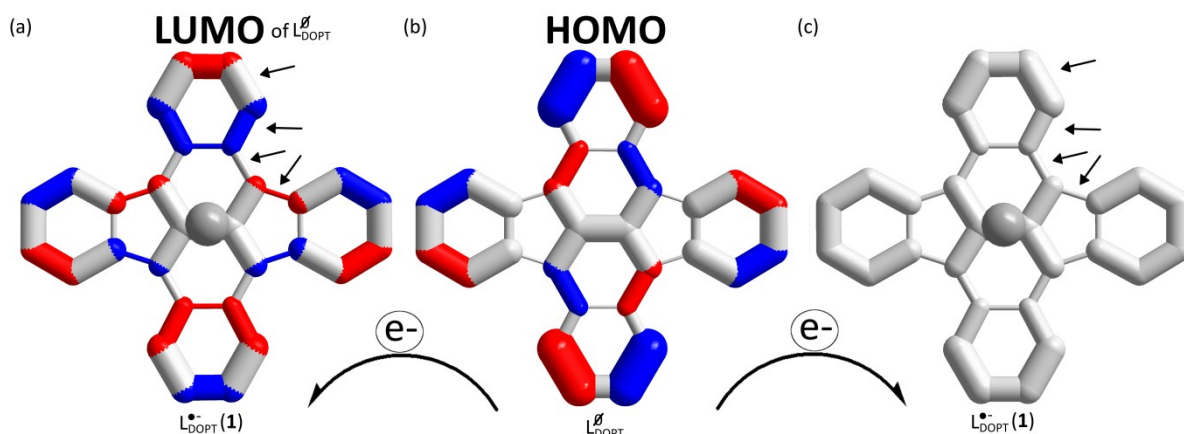


Figure S 5. Illustration of the bond length distribution along the charged perimeter of $[L_{\text{DOPT}}^*]$. (a) The position of the newly occupied LUMO of former L_{DOPT} is indicated in color-mode. (b) Neutral L_{DOPT} is given including the position of its HOMO level given by color-code. (c) Colorless depiction of $[L_{\text{DOPT}}^*]$ in **1** without indication of the LUMO level. (→) Arrows highlight the most significant changes along the core and the tetracenic phenylenes (Pn_{tet}).

3.3 Detailed structural changes in DOPT Di-potassium bis(benzo-15-crown-5-ether) **2**

An analog depiction of the observed structural changes ($\Delta d_{\text{C-C}}$) in the corresponding dianionic state $[L_{\text{DOPT}}^{2-}]$ of compound **2** is given below in Fig. S 4. Table S 5 summarizes the experimentally obtained bond length values ($d(\text{C-C})$) and gives an enlarged side view on the dianionic π -perimeter in **2**.

(a)

(b)

the corresponding X-ray structural data (CCDC 1820792). (bottom) Side view on $[L_{\text{DOPT}}^{2-}]$ in compound **2**.

C(A)-C(B)		d(C-C)	C(A)-C(B)		d(C-C)		
C41	-	C41	138.1	C48	-	C43	147.2
C41	-	C49	141.1	C48	-	C47	140.9
C41	-	C42	142.2	C49	-	C50	144.7
C42	-	C43	144.1	C50	-	C51	141.0
C42	-	C55	144.6	C51	-	C52	139.0
C43	-	C44	140.0	C52	-	C53	139.8
C44	-	C45	139.0	C53	-	C54	139.3
C46	-	C47	139.0	C55	-	C50	146.3
C46	-	C45	139.5	C55	-	C54	140.8
C48	-	C49	144.5				

c
a
b

Table S 5. (top) Bond length values of compound **2** for the charged carbon skeleton in $[L_{\text{DOPT}}^{2-}]$ given in pm. Deviations are omitted for clarity and can be found in

length given in \pm pm referenced to the used starting compound (C 2/c polymorph of neutral L_{DOPT})³.

Figure S 6. (a) Atom numbering scheme of compound **2** based on the allocated atom symbols of the crystal structure data set. (b) Relative change ($\Delta d_{\text{c-c}}$) in bond

An additional visualization of bond length distribution is given below in Fig. S 7. Thick drawing of a C-C bond corresponds to small bond length resp. increased electron concentration and vice versa.

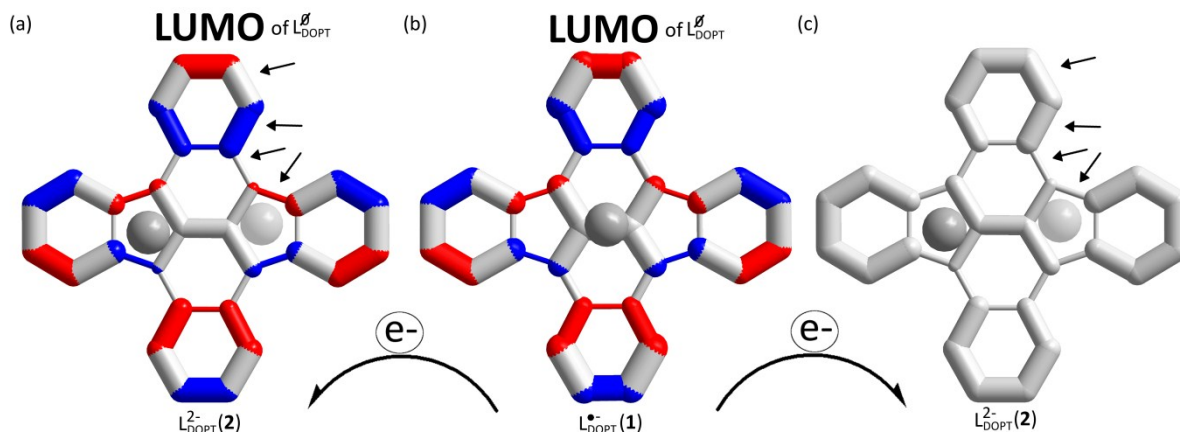


Figure S 7. Illustration of the bond length distribution along the charged perimeter of $[L_{\text{DOPT}}^{2-}]$. (a) The position of the newly occupied LUMO of former L_{DOPT} is indicated in color-mode. (b) Anionic $[L_{\text{DOPT}}^{\bullet-}]$ of **1** is given as reference. (c) Colorless depiction of $[L_{\text{DOPT}}^{2-}]$ of **2** without indication of the LUMO level. (\rightarrow) Arrows highlight the increasing changes along the core and the tetracenic phenylenes (Pn_{tet}) compared to the radical monoanionic species **1**.

4 Comparison of 6 and 7 to the *full naked* anion of DOPT 2

Additionally, full comparison to our earlier presented solvent-shared structures of DOPT as discrete triple-decker structure of rubidium $\{[(18\text{C}6-\kappa^6\text{O})\text{Rb}^+]_2-\mu-(\eta:\eta-L_{\text{DOPT}}^{2-})\}[(18\text{C}6-\kappa^6\text{O})\text{Rb}^+]_2-\mu-(\eta':\eta'-L_{\text{DOPT}}^{2-})\}(\text{THF}_{\text{soliv}})_2\}$ **6** and as 1D-polymeric Cs^+ compound $[\mu-(\eta:\eta-L_{\text{DOPT}}^{2-})_{0.5}(\text{tetraglyme}-\kappa^2\text{O})\text{Cs}^+]_2-\mu-(\eta':\eta'-L_{\text{DOPT}}^{2-})_{0.5}]_n$ **7** is presented (CCDC 1532140 + CCDC 1532140).¹ Deviation in bond length ($\Delta d_{\text{c-c}}$) are given in \pm pm. Both crystallographic different modifications A and B, observed each in **6** as well as in **7**, are faced for completeness (Table S 6). As expected, both solvent-shared ion-pairs clearly deviate from the *full naked* anion **2**.

Table S 6. Summarized variation of the carbon skeletons in both solvent-shared compounds **6+7** including reference values of neutral L_{DOPT} in its monoclinic C 2/c polymorph³ and the *full naked* anion **2**. The bond-allocation a-i follows Fig. S 3a. Compliance with the changes in bond length to compound **2** is marked in dark green. Significant deviations are highlighted in orange. The observed range in bond length deviation ($\Delta d_{\text{c-c}}$) is highlighted in yellow. Values are given in \pm pm.

\rightarrow compound	L_{DOPT}	2	6 ¹		7 ¹	
\rightarrow type	(C 2/c)		(A)	(B)	(A)	(B)
\rightarrow ion(s)	—	2K ⁺	2Rb ⁺	2Rb ⁺	2Cs ⁺	2Cs ⁺
\rightarrow ligands	—	B15C5	18C6	18C6	tetraglyme	tetraglyme
\downarrow bond						
	148.6	-4.1 -4.4	-4.6 -4.8	-5.0 -5.3	-4.9 -5.2	-4.9 -5.2
	142.2 143.0	-1.2 -2.2	-0.9 -2.2	-1.3 -2.0	-0.4 -1.2	-0.9 -2.1
	147.1	-0.8	-2.2	-0.9	-1.4	-1.0
	140.5	-0.7	-1.4	-1.2	-1.9	-1.1

138.2	-0.1	+0.6	-4.7	-0.3	+0.3
139.3 140.0	+1.1 +2.9	-0.3 +1.5	+2.6 +5.2	+1.4 +2.4	+2.2 +3.2
141.0 141.1	+3.5 +3.7	+4.1 +4.7	+2.3 +2.9	+3.2 +3.9	+3.2 +3.6
135.3 135.4	+3.6 +4.0	+2.2 +2.6	+2.2 +3.4	+3.1 +3.2	+3.4 +3.6
143.1	+4.1	+2.8	+4.3	+3.0	+3.2

5 Experimental details

Suitable crystals for structural analysis of **1** and **2** were grown in sealed H-shaped flasks (Fig. S 8) directly from reaction solution under argon at -30°C .

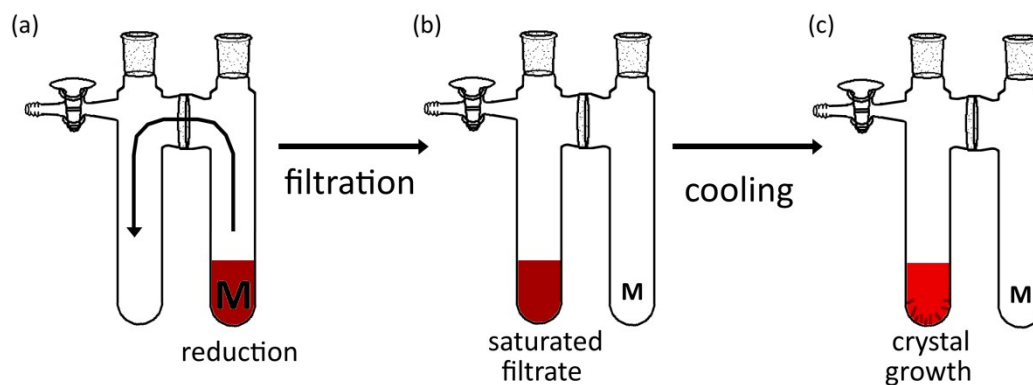


Figure S 8. H-shaped flasks were used for successful synthesis of the highly sensitive complexes **1** and **2**. (a) An excess of the alkaline metal ($M = K$) is placed in one leg of the flame-dried flask, together with predried solvent and purified PAH compound. (b) After sealing of the flask and full conversion to the desired anion at a chosen reaction temperature, separation from excessive metal (M) can be carried out through the embedded fritted glass (P4(P16)) without disturbing the highly sensitive reaction system. (c) At the particular temperature saturated clear solution is obtained, suitable for crystal growth at lower temperatures.

6 Literature

- 1 T. Wombacher, R. Goddard, C. W. Lehmann and J. J. Schneider, *Chem. Commun.*, 2017, **53**, 7030–7033.
- 2 T. Wombacher, R. Goddard, C. W. Lehmann and J. J. Schneider, *Dalt. Trans.*, 2017, **46**, 14122–14129.
- 3 T. Wombacher, A. Gassmann, S. Foro, H. von Seggern and J. J. Schneider, *Angew. Chemie Int. Ed.*, 2016, **55**, 6041–6046.
- 4 R. D. Shannon, *Acta Cryst.*, 1976, **32**, 751–767.
- 5 T. Wombacher, S. Foro and J. J. Schneider, *European J. Org. Chem.*, 2016, 569–578.